Morphological and Calorimetric Studies on the Amorphization Process of Rod-Milled $Al_{50}Zr_{50}$ Alloy Powders

M. SHERIF EL-ESKANDARANY, KIYOSHI AOKI, and KENJI SUZUKI

Amorphous $Al_{50}Zr_{50}$ alloy powders have been prepared by rod-milling technique using mechanical alloying (MA) method. The amorphization and crystallization processes of the alloyed powders were followed by optical microscopy, scanning electron microscopy (SEM), transmission electron microscopy (TEM), X-ray diffraction (XRD), differential thermal analysis (DTA), and differential scanning calorimetry (DSC). The results have shown that the formation of amorphous $Al_{50}Zr_{50}$ alloy powders occurs through three stages, agglomeration, disintegration, and homogenization. At the disintegration stage, the alloyed powders contain many fine layers of Al and Zr. An amorphous phase has been formed at about 880 K as a result of heating these layered particles in a thermal analyzer. The crystalline-to-amorphous transformation at this stage of milling is attributed to a thermally assisted solid-state amorphizing reaction. The present study corroborates the similarity of the amorphization process through the MA with the solid-state interdiffusion reaction in multilayered thin films. The amorphization temperature, T_a, and the activation energy of amorphization, E_a, are 675 and 156 kJ/mol, respectively. In addition, the enthalpy change of amorphization, ΔH_a, was evaluated to be -3.5 kJ/mol. On the other hand, the crystallization temperature, T_x, and enthalpy change of crystallization, ΔH_x, were 1000 K and -68 kJ/mol, respectively.

I. INTRODUCTION

UNTIL recently, amorphous metallic alloys were exclusively prepared by rapid quenching from the liquid or vapor states with very high cooling rates ranging from 10^6 to 10^{12} Ks^{-1}. In 1983, the phenomena of solid-state amorphizing reactions induced by the solid-state interdiffusion of multilayered thin films,[1] hydrogen absorption,[2] and mechanical alloying (MA)[3] have been investigated as a unique technique for preparing several amorphous alloys. In fact, the MA process dates back to 1970, when Benjamin[4] used this process for producing composite metal powders with controlled microstructures. So far, the MA process has been employed for producing many dispersion-strengthened superalloys.[5–9]

In 1983, Koch *et al.*[3] established the synthesis of amorphous $Ni_{60}Nb_{40}$ powders by MA of elemental Ni and Nb powders using a high-energy ball mill. Since then, the MA process *via* ball-milling[10] and/or rod-milling[11,12,13] techniques has been used for preparing various amorphous alloy powders.[14–23] Recently, El-Eskandarany *et al.* have employed this process for producing metal nitrides, such as Fe_2N[24] and nonequilibrium TiN,[25] under purified nitrogen gas flow at room temperature.

The present study reports morphological and calorimetric studies on the amorphization and subsequent crystallization processes of mechanically alloyed $Al_{50}Zr_{50}$ powders produced by the rod-milling technique. The rod-milled alloy powders have been characterized by means of optical metallography, scanning electron microscopy (SEM), transmission electron microscopy (TEM), X-ray diffraction, differential thermal analysis (DTA), and differential scanning calorimetry (DSC).

M. SHERIF EL-ESKANDARANY, Research Associate, Department of Chemical Physics of Non-Crystalline Materials, KIYOSHI AOKI, Associate Professor, Department of Non-Equilibrium Materials, and KENJI SUZUKI, Professor, Department of Chemical Physics of Non-Crystalline Materials, are with the Institute for Materials Research, Tohoku University, Sendai 980, Japan.

Manuscript submitted October 28, 1991.

II. EXPERIMENTAL DETAILS

Pure elemental powders of Al (−325 mesh, 99.999 pct) and Zr (−200 mesh, 99.5 pct) were mixed to give the desired average composition of $Al_{50}Zr_{50}$ in a glove box under a purified argon atmosphere (O_2 and H_2O are less than 1 ppm) and sealed in a cylindrical stainless steel shell (SUS 304, 120 mm in diameter) together with ten stainless steel rods (SUS 304, 10 mm in diameter). The rod-to-powders weight ratio was 30:1. The milling processing was carried out at ambient temperature by mounting the rod mill on a rotator at the rate of 1.4 s^{-1}. The MA experiments were interrupted at regular intervals (starting with 1.8 ks), and a small amount of the rod-milled alloy powders was removed from the vial in the glove box.

The morphology of the alloy powders were studied by optical microscopy, SEM operated at 20 kV, and TEM/energy dispersive X-ray analysis (TEM/EDX) using a 200 kV microscope. The samples for TEM observations were prepared by grinding the alloy powders under ethanol and mounting the suspended powders on a copper microgrid. The structure of the alloy powders was characterized by X-ray diffraction (XRD) using MoKα radiation. Moreover, the thermal properties of the alloys were characterized by means of DTA under an argon atmosphere at a heating rate of 0.33 K/s and DSC in a flow of argon (0.83 ml/s). All the DSC results presented in this study were obtained with heating rates of 0.67 K/s. However, some alloys had been heated at several different heating rates (0.042, 0.083, 0.167, 0.333, 0.500,

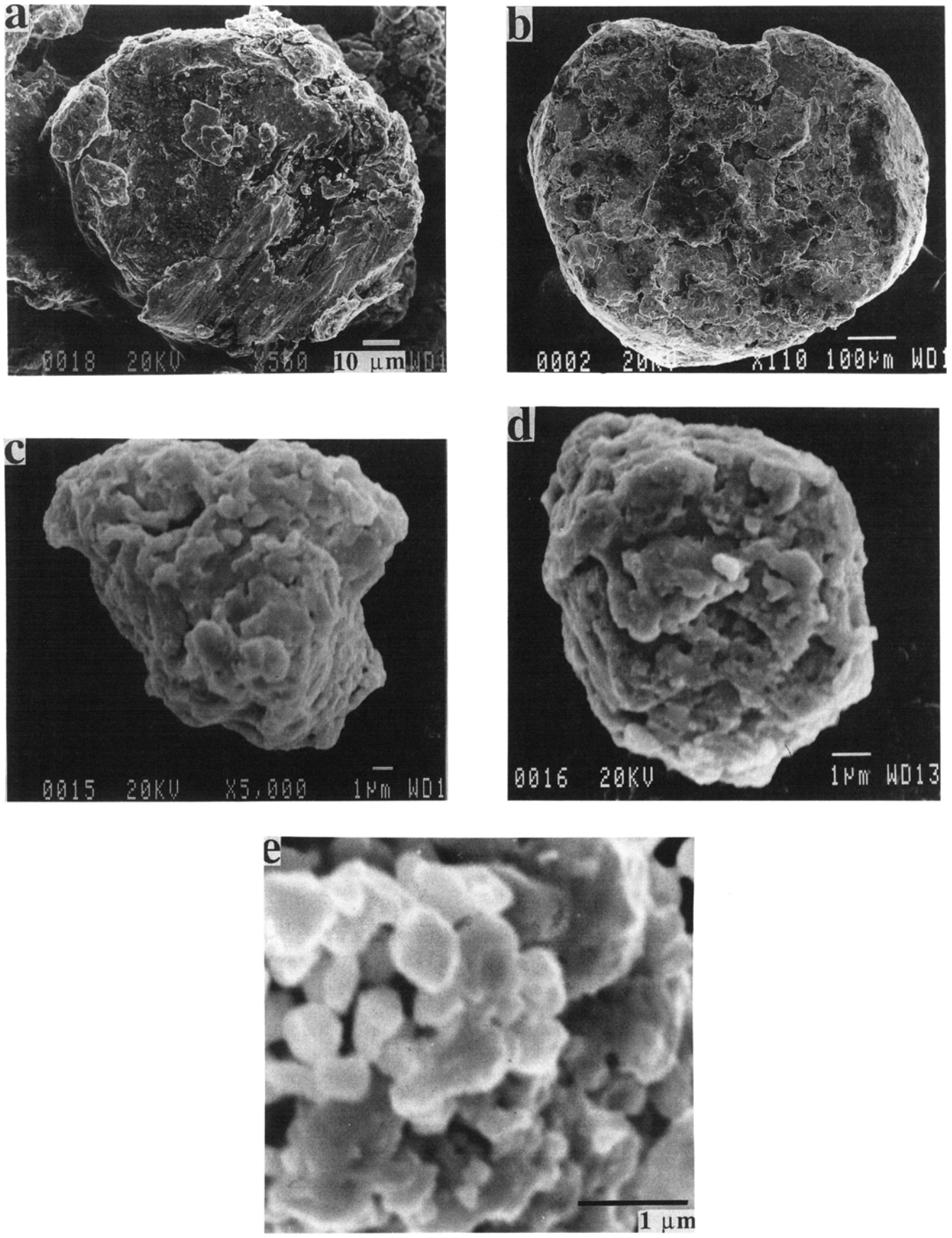

Fig. 1—Scanning electron micrographs of rod-milled $Al_{50}Zr_{50}$ alloy powders after (*a*) 11 ks, (*b*) 43 ks, (*c*) 86 ks, (*d*) 173 ks, and (*e*) 1440 ks of MA time.

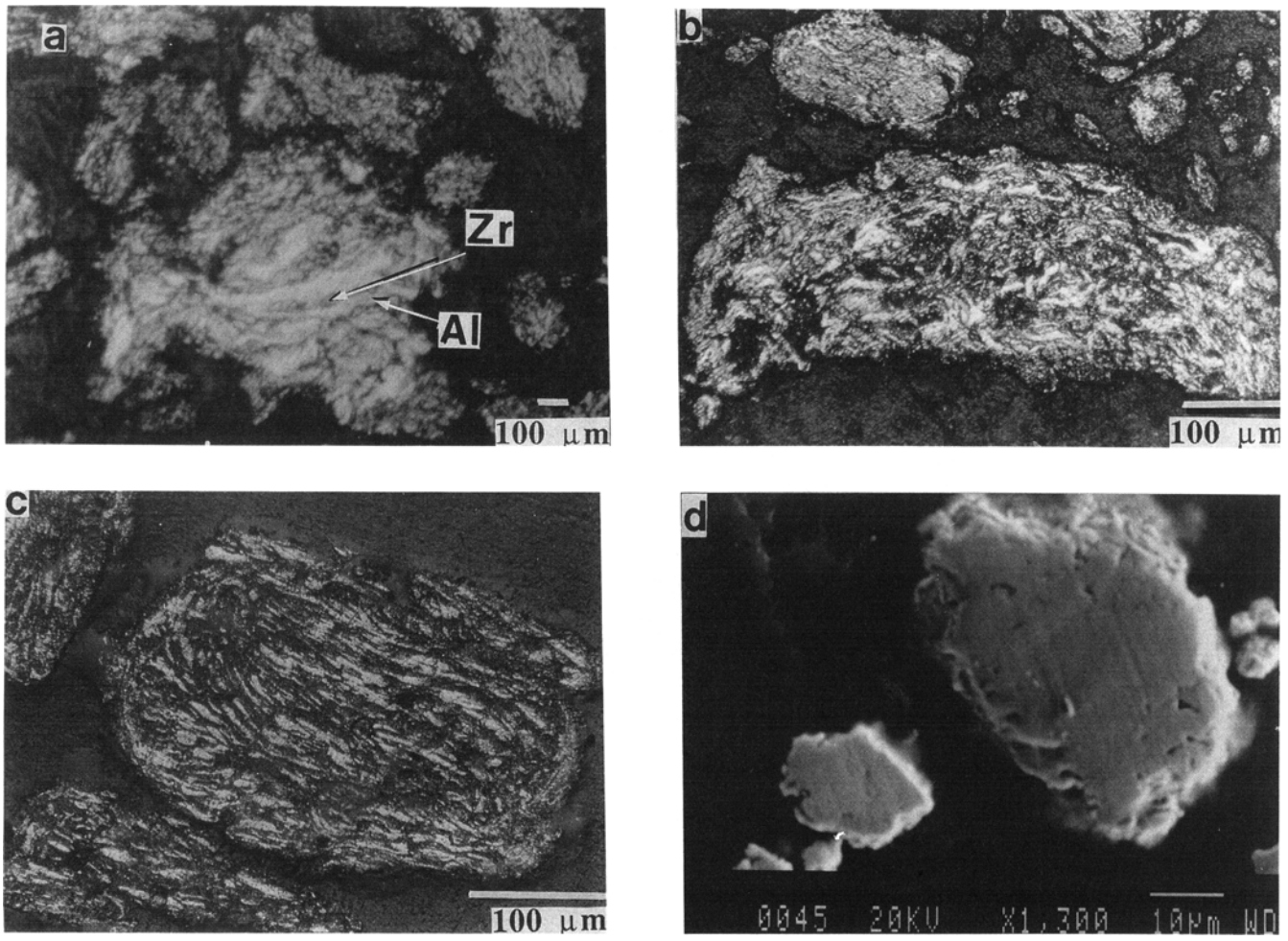

Fig. 2—Cross-sectional view of the polished powder particles of $Al_{50}Zr_{50}$ alloy after (*a*) 11 ks, (*b*) 43 ks, (*c*) 86 ks, and (*d*) 260 ks of MA time.

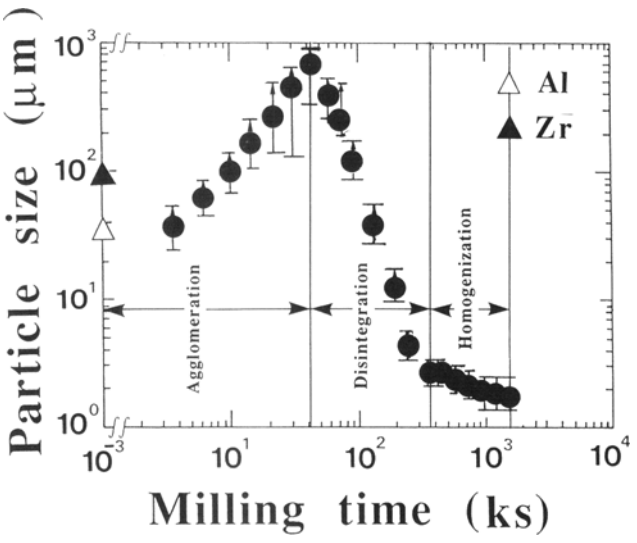

Fig. 3—Particles size distribution of $Al_{50}Zr_{50}$ alloy powders as a function of MA time.

and 0.833 K/s) to determine the amorphization activation energies (E_a) using the Kissinger method.[26] Moreover, the induction coupled plasma (ICP) emission method was used to analyze the contents of Al and Zr and the degree of Fe contamination in the milled powders. The oxygen contamination content in the alloy powders was determined by the helium carrier fusion-thermal conductivity method. After 1440 ks of milling, the iron and oxygen contamination contents in the alloy powders were detected to be 0.65 and 0.30 at. pct, respectively.

III. RESULTS

A. *Morphology*

For the purposes of the present study, detailed SEM observations were performed to determine both of the powders shape and size during the different stages of milling. Figure 1 displays the SEM micrographs of rod-milled $Al_{50}Zr_{50}$ alloy powders after selected milling times. The particles in the first stage of rod milling, exemplified by the 11 and 43 ks alloy powders, are shown in Figures 1(a) and (b), respectively. At the first few kiloseconds of milling (2 to 11 ks), the milling tools are

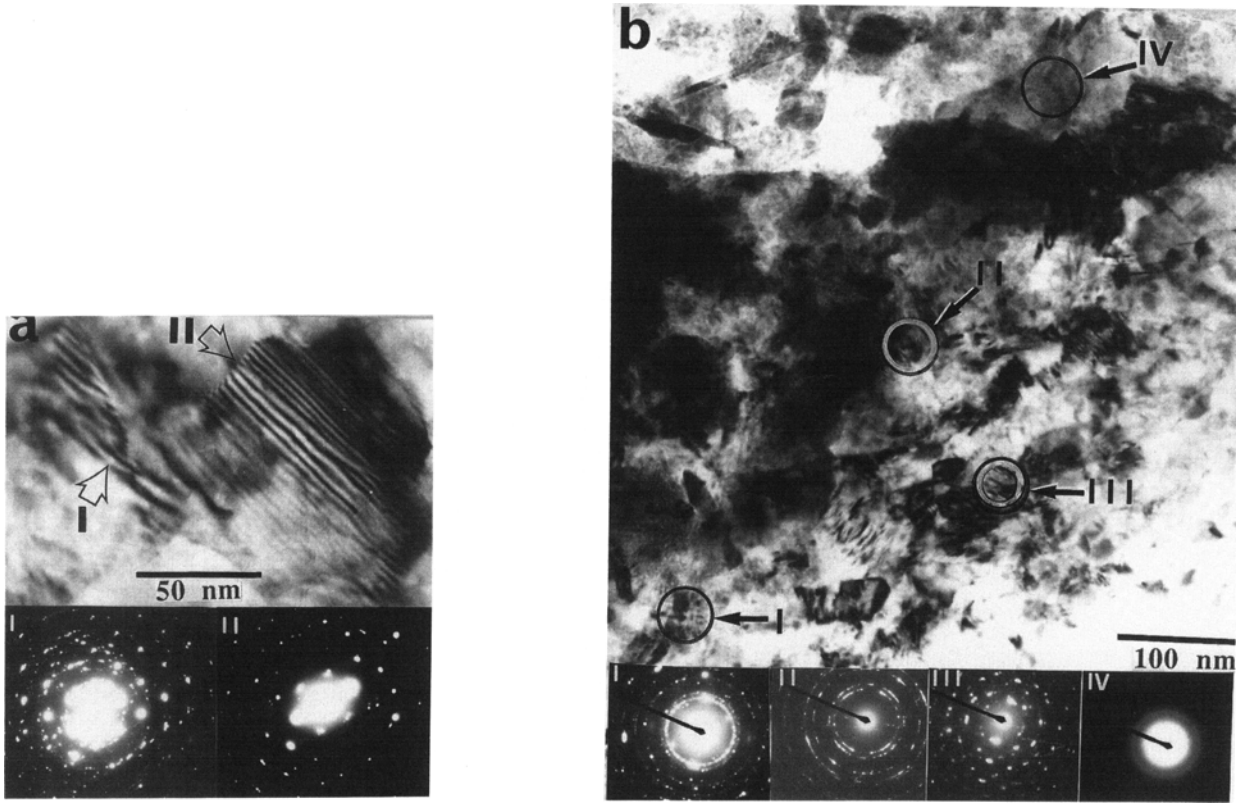

Fig. 4—The bright-field images and the corresponding diffraction patterns of $Al_{50}Zr_{50}$ alloy powders milled for (*a*) 11 ks and (*b*) 173 ks.

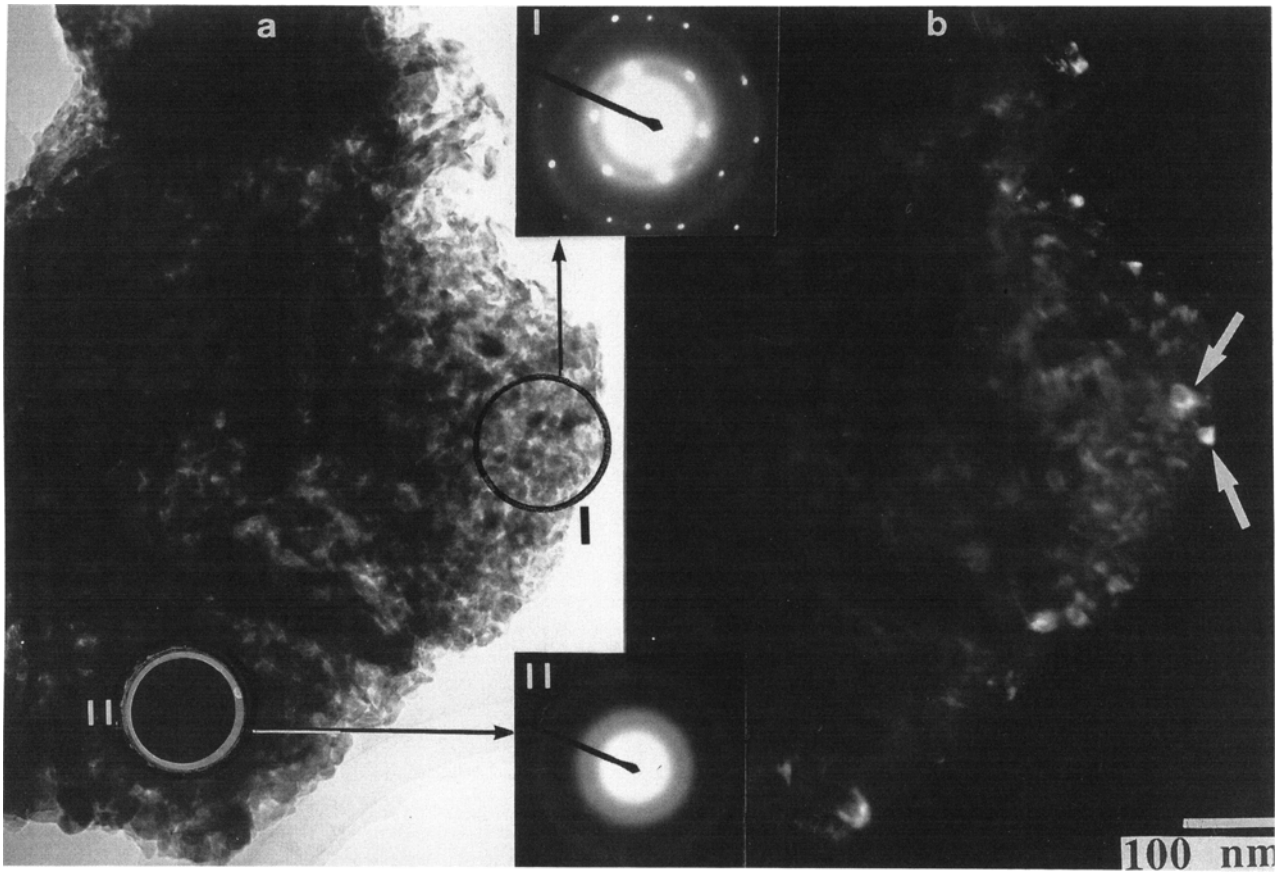

Fig. 5—(*a*) The BFI and (*b*) DFI of mechanically rod-milled $Al_{50}Zr_{50}$ alloy powders after 720 ks of MA time.

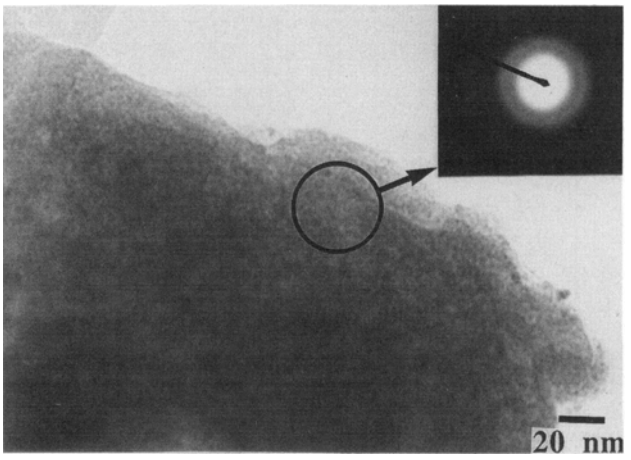

Fig. 6—The BFI of the end product (1440 ks) $Al_{50}Zr_{50}$ alloy powders.

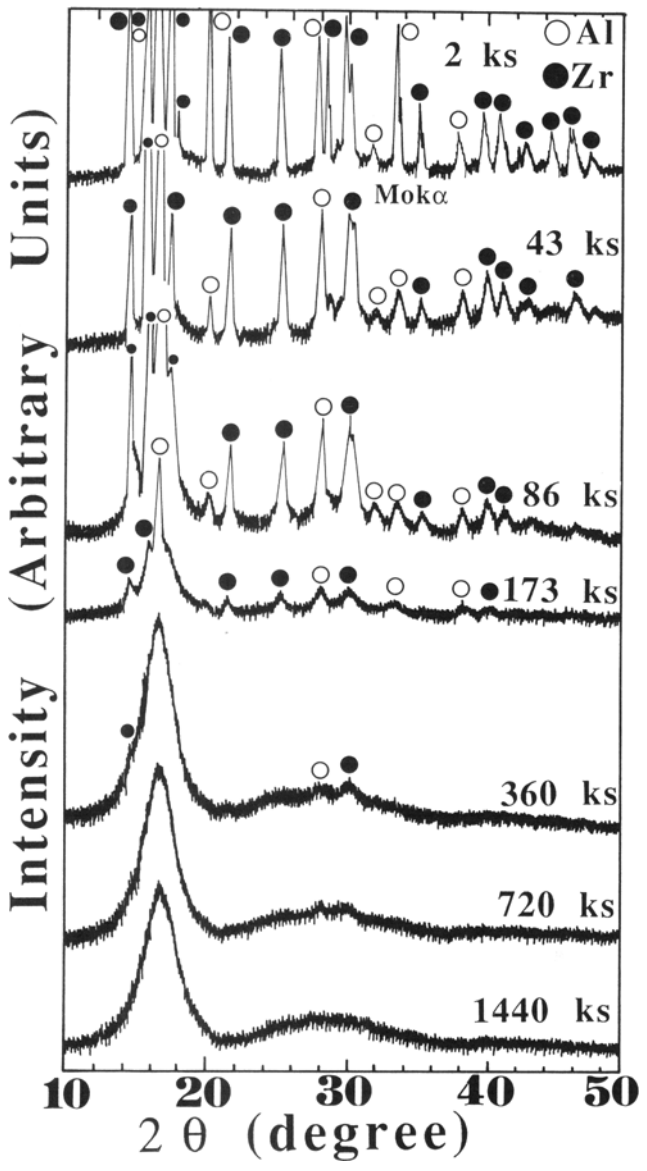

Fig. 7—XRD of mechanically rod-milled $Al_{50}Zr_{50}$ alloy powders as a function of MA time.

coated by thick welded layers of the starting elemental powders. After 11 ks of the MA time, the particles have a globe shape with cabbage or orange skinlike morphology, as shown in Figure 1(a). The optical metallographic examinations of the cross section for polished and etched particles have shown that the powders contain many thick layers of Al and Zr (Figure 2(a)). Obviously, the individual layer has a width of about 100 μm. Further milling (43 ks) leads to the formation of powder particles with greater diameters, as large as 1000 μm, as shown in Figure 1(b). The cross-sectional view for the powder particles shows that the layers become finer, with widths varying from 10 to 25 μm, as shown in Figure 2(b). For longer milling times (86 to 173 ks), the size of the individual particles varies from 10 to 20 μm in diameter, as presented in Figures 1(c) and (d). This is accompanied by a rapid decreasing of the layers' thickness in the individual particles (Figure 2(c)). These layers become hardly visible even by SEM after 260 ks, as shown in Figure 2(d). At the end of the rod-milling process (1440 ks), the powder particles become uniform in their sizes (less than 1 μm in diameter) and have spherical-like morphology, as shown in Figure 1(e). During this stage of milling, the powders' coating-wear is removed from the milling media. This is because the amorphous alloy powders are not ductile and are more brittle than the starting elemental powders.

Figure 3 summarizes the SEM observations of rod-milled $Al_{50}Zr_{50}$ alloy powders at the different stages of milling. Obviously, the MA process performed by the rod-milling technique is classified into three stages, agglomeration, disintegration, and homogenization. In the agglomeration stage (0 to 43 ks), the starting elemental powders of Al and Zr are agglomerated as a result of the repeated cold welding. Moreover, the powders vary widely in size from 100 to 1000 μm. However, at the disintegration stage (43 to 360 ks), which can be also called the amorphization stage (see next paragraph), the agglomerated powder particles are subjected to a continuous fragmentation to form finer powders with sizes less than 10 μm in diameter. Furthermore, this stage of milling provides powder particles with narrow size distribution. The homogenization stage (360 to 1440 ks) refers to the last stage of rod milling, in which all the powders are uniform in shape (almost spherical) and size (less than 1 μm in diameter).

To reveal much more information, the amorphization progress *via* the rod milling technique has also been investigated by TEM and EDX. The TEM/EDX technique provides information on the structure and composition of the powder particles in very small areas (less than 50 nm in diameter). Moreover, this technique allow us to distinguish between the crystalline and the amorphous phase(s) in which SEM is not able to give such information. Figure 4 shows the bright-field images (BFI) and the selected-area diffraction patterns (SADP) of the milled powders at the agglomeration and disintegration stages of the MA process. After 11 ks of rod milling, the powder particles are heavily faulted, characterized by parallel rows of faults which appear as multiple fringes, as shown in Figure 4(a). The SADPs of two regions show a sharp ring-spot pattern that is characteristic of several simultaneously diffracting polycrystalline Al(fcc) (fcc =

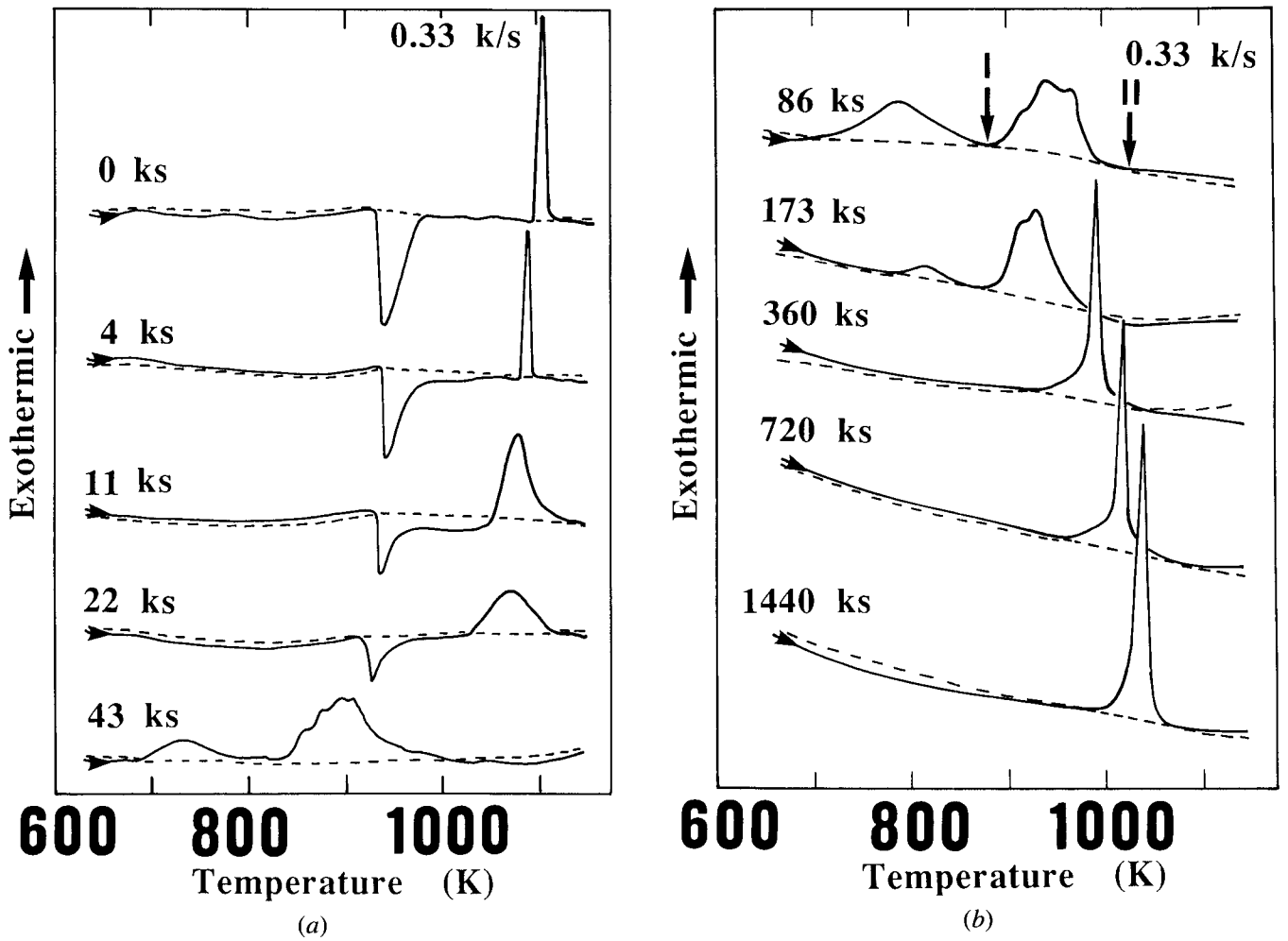

Fig. 8—Typical DTA curves of $Al_{50}Zr_{50}$ alloy powders at the agglomeration stage (*a*) and during the amorphization and homogenization stages (*b*) of milling.

face-centered cubic) and Zr(hcp) (hcp = hexagonal close-packed) (I) and Zr (II). It is worth mentioning that there is no evidence of the formation of an amorphous phase in this stage of milling. Figure 4(b) shows the BFI and the corresponding SADP of four indicated regions for the alloy powders in the disintegration stage of milling (173 ks). The indicated structure in region I corresponds to the polycrystalline Al/Zr crystals, as indexed in SADP (I). On the other hand, the structure of region (II) corresponds to the diffused Al-Zr, as shown in SADP (II). The crystalline reflections visible in the SADP originate from elemental Zr, as shown in region (III) of Figure 4(b). Contrary to this, region (IV) has a fine and somewhat uniform structure, which indicates the existence of an amorphous phase, characterized by a halo diffraction pattern, as shown in SADP (IV). The TEM images of the powder alloys after 260 ks of the MA time are presented in Figure 5(a). Two regions are indicated in the BFI, regions (I) and (II). The SADP of region (I) indicates the formation of an amorphous phase coexisting overlapped with a crystalline phase, characterized by a halo pattern with sharp spot diffraction pattern. In order to determine the origin of this spot pattern, a dark-field image (DFI) was performed, as shown in Figure 5(b). Obviously, very small crystalline particles (less than 20 nm) are observed at the edge, originating from unprocessed Al (fcc). In region (II), however, a clear visible halo pattern is observed, suggesting the formation of an amorphous phase, as shown in SADP (II). The BFI of the end product $Al_{50}Zr_{50}$ alloy powders (1440 ks) is shown in Figure 6. It shows a fine structure without nanocrystalline dimension, suggesting the formation of a complete amorphous phase.

B. *Structure*

X-ray analyses were performed in order to understand the structure of the mechanically alloyed powders formed during the different stages of milling. The XRD patterns of rod-milled $Al_{50}Zr_{50}$ alloy powders are shown in Figure 7 as a function of the MA time. In the early stage of MA (0 to 86 ks), the intensities of the Bragg peaks for pure fcc Al and hcp Zr crystals decrease simultaneously with increasing milling time. At the intermediate stage of the MA (86 to 360 ks), almost all of the minor Bragg peaks from elemental fcc Al and hcp Zr crystals disappear. Further, the major Bragg peaks from pure Al and Zr reflections become wider. In the final stage of the MA time (360 to 1440 ks), a homogeneous amorphous phase is formed, characterized by broad halos and smooth peaks.

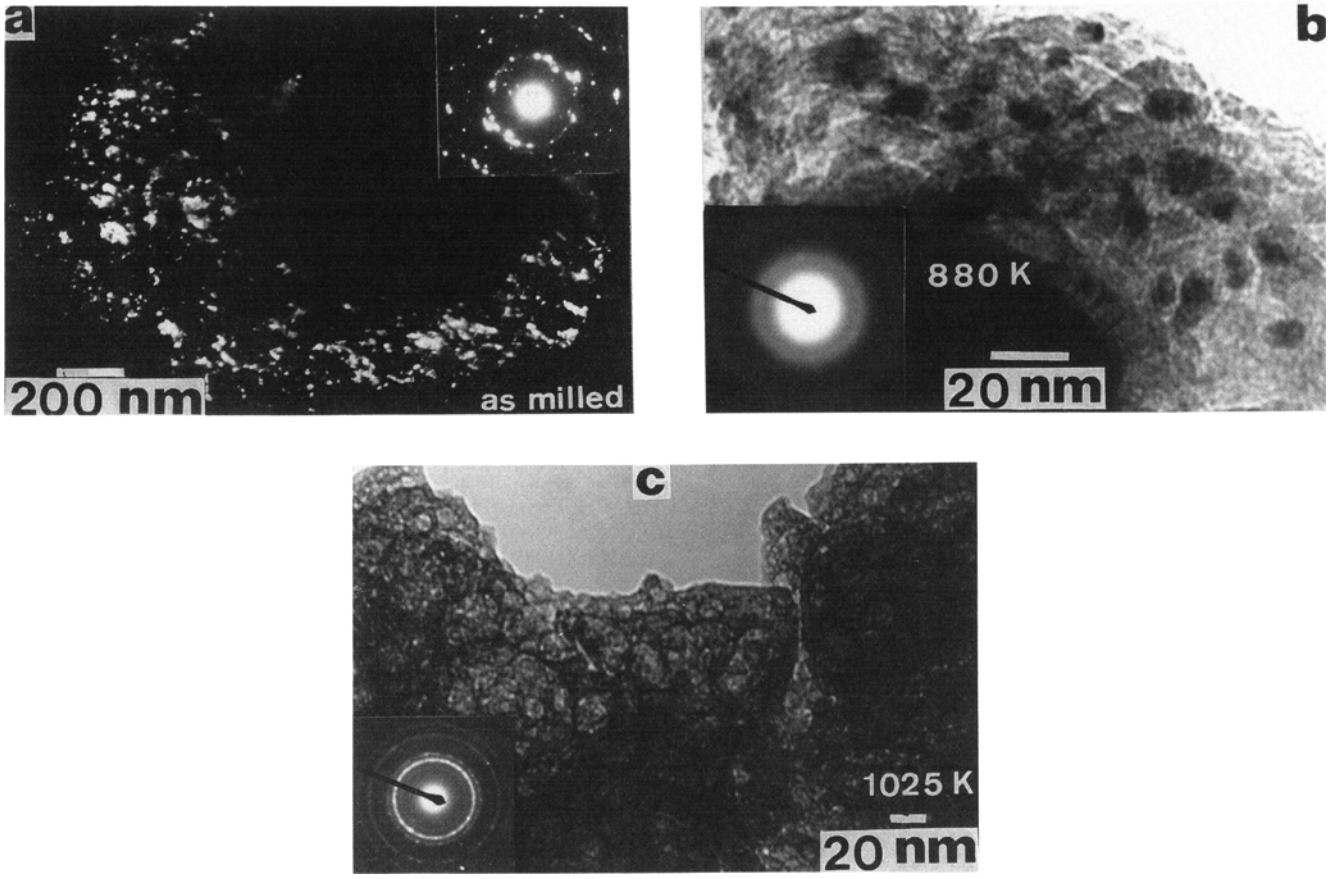

Fig. 9—TEM images and the corresponding diffraction patterns of $Al_{50}Zr_{50}$ alloy powders milled for (*a*) 86 ks, then heated to (*b*) 880 K and (*c*) 1025 K.

C. *Thermal Analysis*

Figure 8 shows the typical DTA curves for $Al_{50}Zr_{50}$ alloy powders as a function of the rod-milling time. All the samples were heated to 1400 K (first run) and cooled down to about 400 K. Then, second heating runs (dashed lines) were performed in order to get a base line. The DTA curves of the alloy powders in the agglomeration stage of milling are shown in Figure 8(a). During this stage of milling, a sharp endothermic peak appears at about 930 K due to the melting of pure Al in the starting material of $Al_{50}Zr_{50}$ powders. The melt then reacts with elemental Zr powders in the mixture, characterized by an exothermic peak appearing above 1100 K. After 43 ks of milling, however, the endothermic and exothermic reaction peaks have already disappeared and two broad exothermic peaks appear. The peak temperature of the first exothermic peak does not change with further milling, as shown in Figure 8(b). Contrary to this, the peak temperature of the second exothermic peak is shifted to the elevated temperature at the amorphization and homogenization stages of milling, as shown in Figure 8(b). Toward the end of the MA time, the second exothermic peak becomes pronounced and sharp and the first exothermic peak disappears.

In order to identify the origin of these exothermic reactions, two samples of 86 ks mechanically alloyed powders were heated separately in the DTA for TEM investigations at (I) and (II), as presented in Figure 8(b). The TEM observations have allowed direct imaging of the phase formation for these samples. Figures 9(a) through (c) show TEM images that were obtained from (a) the as-milled 86 ks alloy powders and as-heated alloy powders up to (b) 880 K and (c) 1025 K, respectively. The DFI of as-milled alloy powders show nanocrystalline particles of Al and Zr, as shown in Figure 9(a). The SADP from several regions shows ring-spot patterns that are characteristic of diffracting polycrystalline Al/Zr. We should emphasize that no evidence for the formation of an amorphous phase could be observed. Contrary to this, the SADP of the sample (II) taken at 880 K indicates the formation of an amorphous phase, characterized by the featureless image and clear halo pattern, as shown in Figure 9(b). Consequently, it is concluded that the first exothermic peak is due to the transformation from the crystalline to amorphous state, *i.e.*, the solid-state amorphizing reaction. The sample (c) taken at 1025 K shows at all regions, without any exceptions, a sharp ring-spot pattern, as shown in Figure 6(c). The ring pattern, which can be indexed as polycrystalline AlZr, is characteristic of crystallization of the amorphous phase.

The DSC curves for the low-temperature range (550 to 800 K) of MA $Al_{50}Zr_{50}$ alloy powders are shown in Figure 10 as a function of the milling time. The DSC was used to get the values of the enthalpy change of amorphization, ΔH_a, the amorphization temperature, T_a,

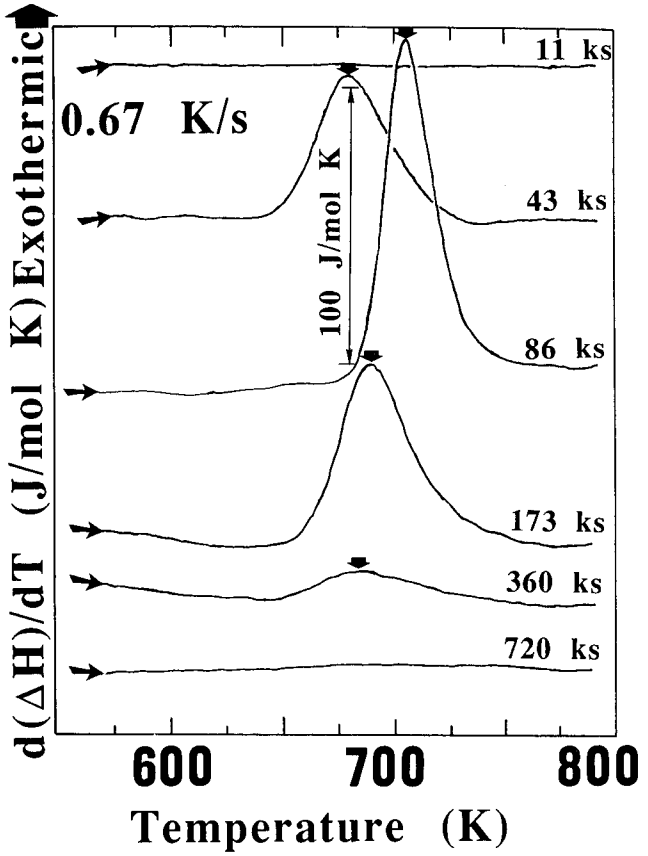

Fig. 10—DSC curves of amorphization peaks for mechanically rod-milled $Al_{50}Zr_{50}$ alloy powders as a function of MA time.

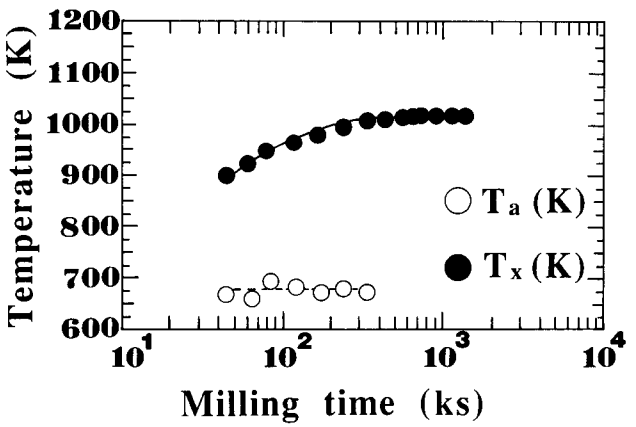

Fig. 11—Effect of MA time on the amorphization temperature, T_a, and the crystallization temperature, T_x, of rod-milled $Al_{50}Zr_{50}$ alloy powders.

Table I. Activation Energy of Amorphization, E_a, for $Al_{50}Zr_{50}$ Alloy Powders at a Selected Milling Time

MA Time (ks)	E_a (kJ/mol)
43	153
86	156
173	152
360	154

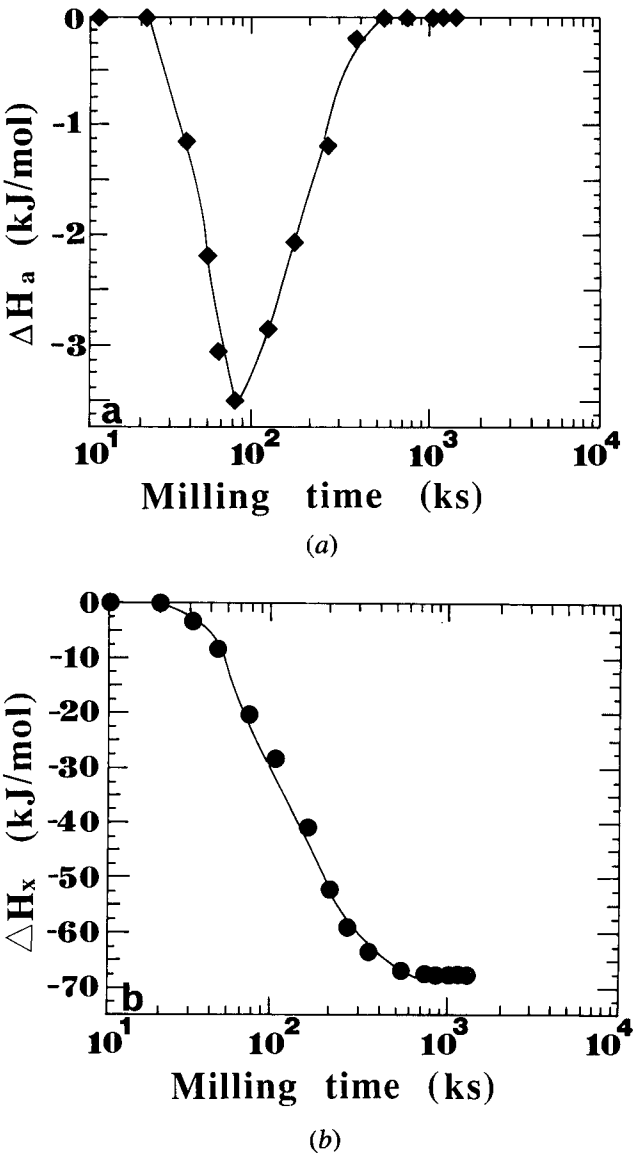

Fig. 12—(*a*) and (*b*) Effect of the MA time on enthalpy change of amorphization, ΔH_a, and the enthalpy change of crystallization, ΔH_x, of rod-milled $Al_{50}Zr_{50}$ alloy powders.

and the activation energy of amorphization, E_a, with more accuracy. The low-temperature exothermic peak, *i.e.*, the amorphization peak, appears at about 680 K after 43 ks of the MA time. After 86 ks of the milling time, this peak becomes more pronounced. Then this amorphization peak gradually disappears to be not remarked after 720 ks of the MA time.

Figure 11 illustrates the T_a (open symbols) and T_x (closed symbols) of mechanically alloyed $Al_{50}Zr_{50}$ powders as a function of the MA time. The value of T_a does not change with increasing the milling time, and the activation energy of amorphization is substantially independent of the milling time, as shown in Table I. However, the crystallization temperature, T_x, increases monotonically with increasing the milling time at the amorphization stage of milling, suggesting a continuous change of the composition of the amorphous phase, and

approaches a saturation value of about 1000 K during the homogenization stage of the MA time.

Figure 12(a) illustrates the change of ΔH_a for mechanically alloyed $Al_{50}Zr_{50}$ powders during the MA process. The value of ΔH_a decreases sharply and approaches a minimum value of about -3.5 kJ/mol after 86 ks of milling. Then, ΔH_a tends to increase monotonically to be almost zero after 540 ks of the MA time. The enthalpy change of crytallization, ΔH_x (the area under the crystallization peak), is shown in Figure 12(b). The value of ΔH_x decreases monotonically with increasing the milling time and approaches a saturation value of about -68 kJ/mol after 540 ks of milling.

IV. DISCUSSION

The results of the present work have shown that the MA process *via* the rod-milling technique consists of three stages of milling. The mechanism of the MA process through each stage of milling will be discussed in this section from the point of view of morphology, structure, and calorimetry.

A. *The Agglomeration Stage*

The agglomeration stage (0 to 43 ks) refers to the first stage of the MA process. After few kiloseconds (4 ks) of the MA time, the powder particles of Al and Zr are blended together without forming any composite particles. At this stage of milling, almost all of the starting materials stick to the surface of the milling media. The particles that do not stick to the milling tools have layered-structure morphology and contain many coarse layers of elemental Al and Zr. Moreover, the composite particles are grown in size to form powder particles of a large diameter as a result of cold welding. At the end of this stage, the particles have a size near 1000 μm in diameter, and the layered-structure morphology becomes clearly visible. During this stage, there is no significant difference in the thermal properties between the alloy powders and the starting materials at 0 ks of milling, as was shown by the DTA measurements. Therefore, the process at the agglomeration stage has the appearance of just blending of the two elemental metal powders. It is worthwhile to say that the particles of this stage vary widely in composition and structure from particle to particle and within the particle itself, suggesting that the alloys of this stage of milling are heterogeneous.

B. *The Disintegration (Amorphization) Stage*

In the disintegration stage (43 to 360 ks), a rapid disintegration of the powder particles occurs, and the particles are reduced sharply in size. Furthermore, all of the particles contain many narrow layers of Al and Zr in a good arrangement as a result of the shear force generated by the rods. The DTA measurements of the alloys at this stage reveal two separate reactions: the first reaction occurs at relatively low temperature (around 675 K), and the second reaction appears at the elevated temperature. The TEM observations have suggested that the first reaction occurs due to a solid-state amorphization reaction between the layers of Al and Zr in the composite particles. However, the second reaction occurred due to subsequent crystallization of the amorphous phase(s). It is worthwhile to say that the formation of the amorphous phase in this stage occurs due to a thermally assisted amorphization[20] conducted by the DTA. As the composite particles contain many layers of Al and Zr, ΔH_a decreases sharply as a consequence of the solid-state diffusion reaction between these layers. On the other hand, ΔH_a increases rapidly with decreasing the number of layers in the particles. When the powder particles do not have any layers of the elemental starting elements, heating them in the DTA does not lead to the formation of any amorphous phases and ΔH_a becomes zero, as will be discussed in Section C.

During this stage, both T_x and $-\Delta H_a$ increase monotonically, suggesting a compositional change and an increase in the volume fraction of the amorphous alloy in the milled powders, respectively. In fact, it is difficult to attribute the formation of the amorphous phase in this stage to the thermal-assisted amorphization only because part of this amorphous phase has occurred mechanically, as was shown in the XRD of the milled alloy powders. Moreover, ΔH_x is larger than ΔH_a, suggesting that two kinds of amorphous phases are crystallized, thermally and mechanically amorphous phases. Thus, the crystallization process in this stage contains the crystallites of the as-milled amorphous phase(s) plus the crystallites of as-heated amorphous phase(s).

The amorphization stage is unique in that an amorphous alloy free from iron and oxygen contaminations can be obtained just by heating the layered particles to about 880 K without further milling. However, the formed amorphous *via* the DTA method is not homogeneous, indicated by the broad crystallization peaks, as shown in Figure 8. Moreover, this amorphous phase(s) is not stable and has a low thermal stability, suggested by the low values of ΔH_a and T_x, as shown in Figure 12. Therefore, further milling is required to improve the thermal properties of the amorphous alloy and to form a stable and homogeneous amorphous alloy (see Section C).

C. *The Homogenization Stage*

The homogenization stage (360 to 1440 ks) is the last stage of milling in which the solid-state amorphizing reaction takes place homogeneously to form a uniform amorphous phase. Toward the end of this stage, the amorphous phase has XRD patterns with broad and smooth peaks. It is worth noting that the layered-structure morphology, as examined by cross-sectional SEM of the particles, had already disappeared. Therefore, the first exothermic peaks which are related to a thermally assisted solid-state amorphizing are absent, indicating that the formation of the amorphous phase occurs due to a mechanical driving force. During this stage, the amorphous alloy powders crystallize through a single sharp exothermic peak, suggesting that the formed amorphous phase is single and homogeneous in composition. In fact, the milling process at this stage occurs fast and much more homogeneously than that at the last two stages. This is demonstrated by the nearly constant values of the particle size, T_x and ΔH_x.

V. CONCLUSIONS

The goal of the present article has been to provide a systematic evolution of the mode of amorphization and crystallization for mechanically rod-milled $Al_{50}Zr_{50}$ alloy powders. The present work allows the following interpretations:

1. The amorphization process takes place in three distinct stages, agglomeration, disintegration, and homogenization. The end product of each stage varies widely from stage to stage in the structure, morphology, and thermal properties.
2. At the amorphization stage of MA, heating the alloy powders to 880 K leads to the formation of an amorphous phase by thermally assisted amorphization reaction.
3. The enthalpy change of amorphization, ΔH_a, of 86 ks alloy powders was found to be -3.5 kJ/mol.
4. The amorphization temperature, T_a, and the activation energy of amorphization, E_a, are independent of the MA time and almost have the same value of about 675 K and 156 kJ/mol, respectively.
5. The crystallization temperature, T_x, and the heat of the enthalpy change of crystallization, ΔH_x, of amorphous $Al_{50}Zr_{50}$ alloy powders milled for 1440 ks were determined to be 1000 K and -68 kJ/mol, respectively.

ACKNOWLEDGMENTS

The authors are indebted to Professor K. Sumiyama and Professor E. Ivanov for helpful discussions. The authors are also grateful to Professor H. Nakajima, Dr. Y. Minonishi, and Dr. S. Yano for useful comments and suggestions. The authors wish to thank Dr. Haruko Itoh at Sun Frontier Technology Co. Ltd., Moniwadai, Sendai, Japan, for her kind support during SEM observations. This work was partially supported by the Ministry of Education, Science and Culture, Grant-in-Aid for Developmental Scientific Research (B) (03555139) and Grant-in-Aid for Cooperative Research (03302053).

REFERENCES

1. R.B. Schwarz and W.L. Johnson: *Phys. Rev. Lett.*, 1983, vol. 51, pp. 415-18.
2. X.L. Yeh, K. Samwer, and W.L. Johnson: *Appl. Phys. Lett.*, 1983, vol. 42, pp. 242-44.
3. C.C. Koch, O.B. Cavin, C.G. McKamey, and J.O. Scarbourgh: *Appl. Phys. Lett.*, 1983, vol. 43, pp. 1017-19.
4. J.S. Benjamin: *Metall. Trans.*, 1970, vol. 1, pp. 2943-51.
5. I.G. Wright and B.A. Wilcox: *Metall. Trans.*, 1974, vol. 5, pp. 957-60.
6. G.H. Gessinger: *Metall. Trans. A*, 1976, vol. 7A, pp. 1203-09.
7. J.S. Benjamin: *Sci. Am.*, 1976, vol. 40, pp. 234-40.
8. J.S. Benjamin and M.J. Bomford: *Metall. Trans. A*, 1977, vol. 8A, pp. 1301-05.
9. P.S. Gilman and W.D. Nix: *Metall. Trans. A*, 1981, vol. 12A, pp. 813-24.
10. M. Sherif El-Eskandarany, K. Aoki, H. Itoh, and K. Suzuki: *J. Less-Common Met.*, 1991, vol. 169, pp. 235-44.
11. M. Sherif El-Eskandarany, K. Aoki, and K. Suzuki: *J. Less-Common Met.*, 1990, vol. 167, pp. 113-18.
12. M. Sherif El-Eskandarany, K. Aoki, and K. Suzuki: *J. Japan Soc. Powder Powder Metallurgy (JSPM)*, 1991, vol. 38 (1), pp. 59-62.
13. M. Sherif El-Eskandarany, K. Aoki, and K. Suzuki: *Proc. Int. Symp. on Mechanical Alloying (ISMA)*, Kyoto, Japan, May 7–10, 1991, P.H. Shingu, ed., Trans Tech Publications, Aedermannsdorf, Switzerland; also *Mater. Sci. Forum*, 1992, vols. 88–90, pp. 81-88.
14. R.B. Schwarz, R.R. Petrich, and C.K. Saw: *J. Non-Cryst. Solids*, 1985, vol. 76, pp. 281-301.
15. J. Eckert, L. Schultz, E. Hellstern, and K. Urban: *J. Appl. Phys.*, 1988, vol. 64, pp. 3224-28.
16. A. Calka and A.P. Radlinski: *Scripta Metall.*, 1989, vol. 23, pp. 1497-1501.
17. M. Sherif El-Eskandarany, F. Itoh, K. Aoki, and K. Suzuki: *J. Non-Cryst. Solids*, 1990, vol. 117–118, pp. 729–32.
18. Y.S. Cho and C.C. Koch: *Mater. Sci. Eng.*, 1991, vol. A141, pp. 139-48.
19. M. Sherif El-Eskandarany, K. Aoki, and K. Suzuki: *Scripta Metall.*, 1991, vol. 25, pp. 1695-1700.
20. M. Sherif El-Eskandarany, K. Aoki, and K. Suzuki: *J. Appl. Phys.*, 1992, vol. 71 (6), pp. 2924-30.
21. M. Sherif El-Eskandarany, H. Suzuki, K. Aoki, and K. Suzuki: *J. Japan Soc. Powder Powder Metallurgy (JSPM)*, 1991, vol. 38 (7), pp. 96-101.
22. M. Sherif El-Eskandarany, K. Aoki, and K. Suzuki: *J. Alloys Compounds*, 1991, vol. 177, pp. 229-44.
23. M. Sherif El-Eskandarany, K. Aoki, and K. Suzuki: *Proc. 5th Int. Conf. on the Structure of Non-Crystalline Materials (NCM 5)*, Akiu-Sendai, Japan, Sept. 2–6, 1991, K. Suzuki, ed., in press.
24. M. Sherif El-Eskandarany, K. Sumiyama, K. Aoki, and K. Suzuki: in *Proc. Int. Symp. on Mechanical Alloying (ISMA)*, Kyoto, Japan, May 7–10, 1991, P.H. Shingu, ed., Trans Tech Publications, Aedermannsdorf, Switzerland; also *Mater. Sci. Forum*, 1992, vols. 88–90, pp. 801-08.
25. M. Sherif El-Eskandarany, K. Sumiyama, K. Aoki, and K. Suzuki: *J. Mater. Res.*, 1992, vol. 7 (4), pp. 888-93.
26. H.E. Kissinger: *Analyt. Chem.*, 1957, vol. 29, pp. 1702-06.